# Magnetoexcitons in planar type-II quantum dots in a perpendicular magnetic field

K. L. Janssens,* B. Partoens,† and F. M. Peeters‡
*Departement Natuurkunde, Universiteit Antwerpen (UIA), Universiteitsplein 1, B-2610 Antwerpen, Belgium*
(Received 20 March 2001; revised manuscript received 25 June 2001; published 27 September 2001)

We study an exciton in a type-II quantum dot, where the electron is confined in the dot, but the hole is located in the barrier material. The exciton properties are studied as a function of a perpendicular magnetic field using a Hartree-Fock mesh calculation. Our model system consists of a planar quantum disk. Angular momentum ($l$) transitions are predicted with increasing magnetic field. We also study the transition from a type-I to a type-II quantum dot which is induced by changing the confinement potential of the hole. For sufficiently large magnetic fields a reentrant behavior is found from $l_h=0$ to $l_h\neq 0$ and back to $l_h=0$, which results in a transition from type II to type I.

DOI: 10.1103/PhysRevB.64.155324 PACS number(s): 73.21.La, 71.35.Ji, 85.35.Be

## I. INTRODUCTION

Self-assembled quantum dots[1] have become the subject of intensive research, both theoretically and experimentally, since their first realization in the early 1990s.[2–5] The reason for this large interest is, e.g., due to their possible applications in optoelectronic devices, such as quantum dot lasers. The formation of this type of dots by the Stranski-Krastanow growth mode requires two semiconductor materials with a considerable lattice mismatch of typically 5%. Many experimental[6–10] and theoretical[11–15] works are devoted to type-I structures, e.g., InAs/GaAs or InAlAs/AlGaAs, where both electrons and holes are located inside the quantum dots.

Also very interesting, though yet less studied, are the type-II quantum dots, where the quantum dot forms an antidot for one of the types of carriers, e.g., for the holes in typically the InP/GaInP system or the electrons in, e.g., GaSb/GaAs. Landau level formation in strongly optically populated type-II dots was observed by Nomura *et al.*[16] in the photoluminescence spectra at high magnetic fields. Other magnetophotoluminescence experiments on vertically stacked InP quantum dots were performed by Hayne *et al.*[17] Sugisaki *et al.*[18] studied the magnetic field effects in a single InP dot. The optical recombination spectrum and the carrier dynamics of the GaSb/GaAs system have been studied experimentally by Hatami *et al.*[19]

Whereas the type-I system has been the subject of many theoretical works, only few theoretical studies have paid attention to the type-II system. Pryor *et al.*[20] studied the electronic structure of InP/GaInP, using a strain-dependent $\mathbf{k}\cdot\mathbf{p}$ Hamiltonian. Also for InP/GaInP dots, Nomura *et al.*[21] performed a theoretical calculation of the Landau levels in a high magnetic field by solving the Hartree equations self-consistently. Using the Hartree-Fock approximation, the binding energy of excitons, charged excitons, and biexcitons was studied by Lelong *et al.*[22] in GaSb/GaAs dots at zero magnetic field. The magnetoexciton in a GaSb/GaAs dot was investigated by Kalameitsev *et al.*[23] They found transitions of the angular momentum with increasing magnetic field.

In the present paper, we focus our attention on the properties of a single exciton which is bound by the Coulomb interaction in a *model* type-II quantum dot. We will take material parameters of the InP/GaInP system. Furthermore, we apply an external magnetic field in the growth direction, i.e., $\mathbf{B}=B\mathbf{e}_z$. Including a magnetic field allows us to investigate the transition region from exciton confinement due to the Coulomb potential to a confinement which is due to the magnetic field. As a model system we take a planar quantum disk and assume that the particles are confined in a plane in the $z$ direction. Strain effects are neglected in this model system.

In our model type-II quantum dot the electron is confined in the dot and the hole sits outside. The corresponding geometry is shown in Fig. 1. The reverse confinement situation will lead to the same physics. As we do not take the confinement effects due to strain into account, the hole is only confined because of the Coulomb attraction to the electron. As we have no *a priori* knowledge about the width of the hole wave function it is difficult to choose good basis functions for the expansion of the hole wave function. Therefore, we solved the Hartree-Fock (HF) equations on a grid, which allows very flexible solutions, in principle, of arbitrary shape. With the same motivation, similar Hartree-Fock mesh calculations were recently used in atomic physics.[24]

As confinement potential, we take hard walls of finite height. By varying the hole confinement potential, we can

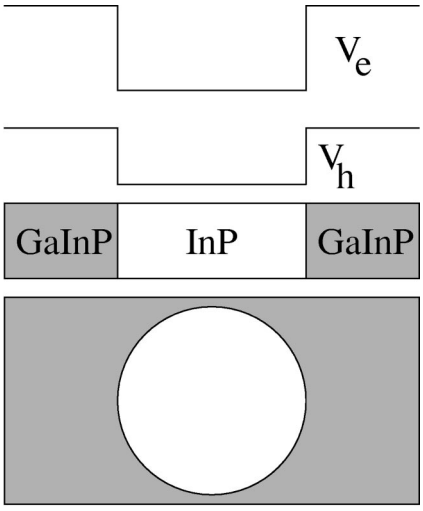


FIG. 1. The geometry of the system under consideration, with side and top views.

 ©2001 The American Physical Society

study the transition from a type-I structure (i.e., the hole is confined in the dot) to a type-II structure (i.e., the dot is a barrier for the hole). We show that for small antidots the attraction of the hole to the electron is stronger than the barrier energy and the system is still type I. Increasing the barrier height and/or the size of the dot induces a transition to a type-II system. Furthermore, we found angular momentum transitions with increasing magnetic field. For large enough magnetic fields (depending on the height of the potential barrier), we find a new reentrant behavior to the zero angular momentum state.

The paper is organized as follows. In Sec. II, we describe briefly our theoretical model. The numerical results are presented in Sec. III. In Sec. III A, we discuss the effect of a varying magnetic field and explain the origin of the angular momentum transitions. Section III B deals with the transition from a type-I to a type-II system. Section III C is dedicated to the reentrant behavior. In Sec III D, we present the results for the excitation spectrum. Our results are summarized in Sec. IV. In the Appendix, we discuss in more detail the method we used for the calculation of the Hartree integral.

## II. THEORETICAL MODEL

The energies and wave functions are obtained by solving the following HF single-particle equations in the effective mass approximation (with $m_e$ and $m_h$ the effective electron and hole masses, respectively, $r_{e,h}=\sqrt{x_{e,h}^2+y_{e,h}^2}$, $\omega_{c,e}=eB/m_e$, and $\omega_{c,h}=eB/m_h$):

$$\left[-\frac{\hbar^2}{2m_e}\frac{1}{r_e}\frac{\partial}{\partial r_e}\left(r_e\frac{\partial}{\partial r_e}\right)+\frac{\hbar^2}{2m_e}\frac{l_e^2}{r_e^2}+\frac{l_e}{2}\hbar\omega_{c,e}+\frac{1}{8}m_e\omega_{c,e}^2r_e^2+V_e(r_e)-\frac{e^2}{4\pi\epsilon}\int\frac{\rho_h(r')}{|\mathbf{r}-\mathbf{r}'|}d\mathbf{r}'\right]\psi_e(r_e)=\epsilon_e\psi_e(r_e), \quad (1a)$$

$$\left[-\frac{\hbar^2}{2m_h}\frac{1}{r_h}\frac{\partial}{\partial r_h}\left(r_h\frac{\partial}{\partial r_h}\right)+\frac{\hbar^2}{2m_h}\frac{l_h^2}{r_h^2}-\frac{l_h}{2}\hbar\omega_{c,h}+\frac{1}{8}m_h\omega_{c,h}^2r_h^2+V_h(r_h)-\frac{e^2}{4\pi\epsilon}\int\frac{\rho_e(r')}{|\mathbf{r}-\mathbf{r}'|}d\mathbf{r}'\right]\psi_h(r_h)=\epsilon_h\psi_h(r_h), \quad (1b)$$

where we made use of the axial symmetry by taking $\Psi_e(r_e,\varphi_e)=e^{il_e\varphi_e}\psi_e(r_e)$ and $\Psi_h(r_h,\varphi_h)=e^{il_h\varphi_h}\psi_h(r_h)$, and where the densities $\rho_e(r')$ and $\rho_h(r')$ are given by, respectively, $|\Psi_e(r_e,\varphi_e)|^2$ and $|\Psi_h(r_h,\varphi_h)|^2$. The Hartree-Fock equations were solved using a finite-difference scheme. More details about the implementation of this finite-difference scheme can be found in Refs. 25 and 15. Note that there are no exchange terms as we only consider a single electron and a single hole. However, these equations can still be called HF as the self-interaction is excluded. As confinement potentials we take hard walls of finite height:

$$V_{e,h}(r_e,r_h)=\begin{cases}V_{e,h}, & r_{e,h}>R,\\ 0, & \text{otherwise},\end{cases} \quad (2)$$

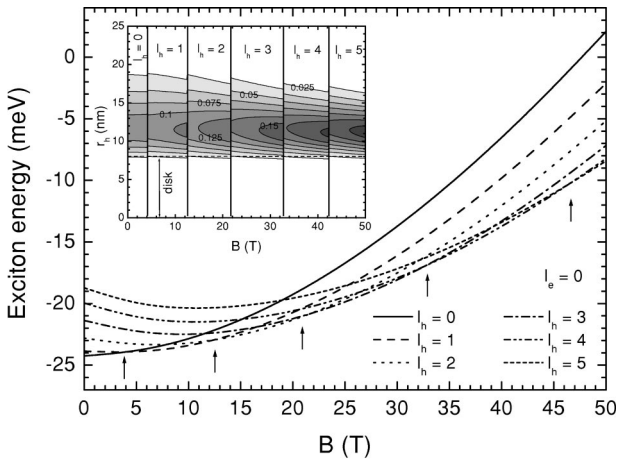


FIG. 2. The exciton energy as a function of the magnetic field, for $R=8$ nm, $V_e=250$ meV, and $V_h=-50$ meV. The successive $l_h$ transitions are indicated by arrows. The inset shows a contour plot of the square of the hole wave function as a function of the magnetic field.

with $R$ the radius of the disk, and where we took $V_e$ positive and $V_h$ negative. Note that the only good quantum number is the total angular momentum in the $z$ direction, defined by $L=l_e+l_h$.

These equations must be solved self-consistently, which is done iteratively. We start with the free electron solution because in the absence of any Coulomb interaction only the free electron is confined. The Hartree integrals are integrated numerically,

$$\int\frac{\rho(r')}{|\mathbf{r}-\mathbf{r}'|}d\mathbf{r}'=4\int\frac{\rho(r')r'}{r+r'}\mathcal{K}\left(\frac{4rr'}{(r+r')^2}\right)dr', \quad (3)$$

where $\mathcal{K}(x)$ is the complete elliptic integral of the first kind. More details about the calculation and numerical implementation of this integral are given in the Appendix.

After convergence, the total energy is given by

$$E_{\text{exciton}}=\epsilon_e+\epsilon_h+\frac{e^2}{4\pi\epsilon}\int\int\frac{\rho_e(r)\rho_h(r')}{|\mathbf{r}-\mathbf{r}'|}d\mathbf{r}d\mathbf{r}'. \quad (4)$$

The contribution of the correlation to the total energy is neglected in HF, but for the self-assembled quantum dots, it is expected to be less than 2%.[12]

## III. RESULTS

### A. Angular momentum transitions

First, we calculated the ground-state energy of the exciton as a function of the external magnetic field. We took the following parameters: $m_e=0.077m_0$, $m_h=0.6m_0$, $V_e=250$ meV, $V_h=-50$ meV, and $\epsilon=12.61$, which are typical for the InP/GaInP system,[20] and consider a dot of radius $R=8$ nm.[17] Our numerical results are depicted in Fig. 2 and show that the exciton ground state exhibits transitions of the angular momentum $l_h$ as a function of the magnetic field (indicated by the arrows). These changes in angular momen-

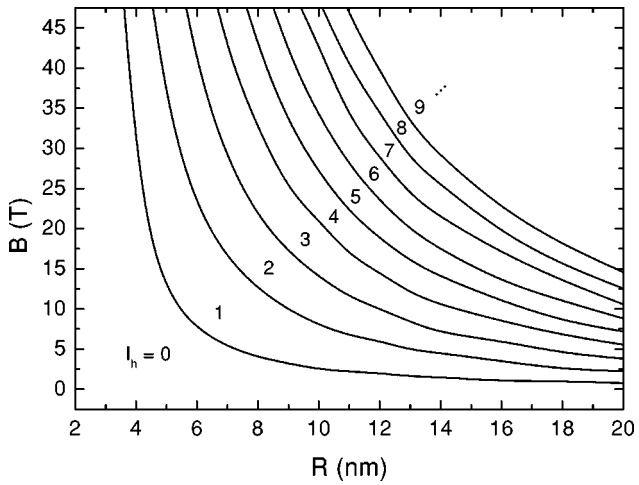


FIG. 3. Phase diagram of the $l_h$ transitions as a function of magnetic field $B$ and disk radius $R$, for $V_h=-50$ meV.

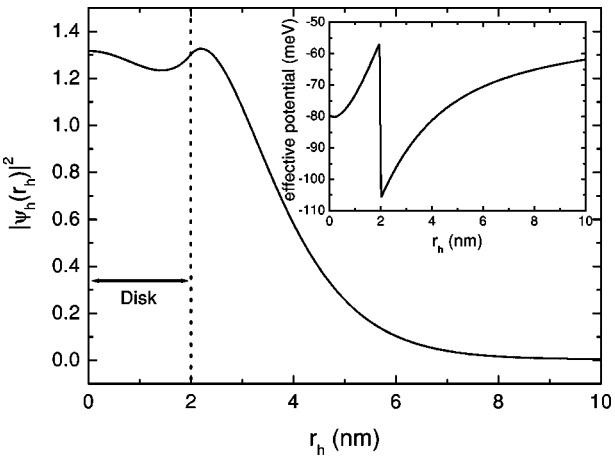


FIG. 4. Hole wavefunction for $R=2$ nm and $V_h=-50$ meV, at $B=0$ T. The inset shows the effective confinement potential for the hole.

tum of the ground state are *not* present in type-I dots and are a direct consequence of the fact that we are dealing with type-II dots. For the hole, the disk acts as a barrier and by increasing the magnetic field the hole is pushed closer to the disk boundary which leads to an increase of the hole potential energy. For a certain magnetic field it is for the hole energetically more favorable to jump to a higher $l_h$ state, which brings the hole farther away from the disk interface. This is also demonstrated in the inset of Fig. 2, where a contour plot of the density of the hole wave function is shown as a function of both the magnetic field and the radial position. It is apparent that the hole is located close to the disk, even at zero magnetic field, and that with increasing magnetic field the hole is pushed closer to the border of the disk. At the angular momentum transitions the hole is spread out a little more and jumps a distance away from the disk interface. But note that on average the hole is pushed closer to the disk boundary and its width decreases with increasing magnetic field. For the present case we find five transitions for a magnetic field up to $B=50$ T.

The magnetic field values at which the angular momentum transitions occur will depend on the disk radius $R$. Figure 3 shows a phase diagram of the $l_h$ transitions as a function of the magnetic field $B$ and the disk radius $R$, for the InP parameters used above. With increasing disk radius, the transitions shift to lower magnetic field values. This can be understood as follows: for larger disks, a smaller magnetic field is needed to push the hole close to the border of the disk and to induce an angular momentum transition.

Another way to understand the angular momentum transitions is as follows. The hole is spatially confined into a ringlike area, and if we make the extreme simplification of a zero width ring, the hole energy is given by

$$E_h=\frac{\hbar^2}{2mR^2}\left(l_h-\frac{\phi}{\phi_0}\right)^2, \tag{5}$$

from which it is clear that the ground state exhibits angular momentum transitions each time the flux through the ring $\phi$ equals $(l_h+1/2)\phi_0$ with $\phi_0=hc/e$ the quantum of flux.

### B. Type-II to type-I transitions

In Fig. 4 we give a closer look at the hole wave function for a very small disk $R=2$ nm, $V_h=-50$ meV, and $B=0$ T, and we find that, even without a magnetic field, the hole is partially situated inside the quantum disk. This is a remarkable effect, as from the shape of the effective potential, defined by the sum of the confinement potential and the Hartree potential (inset of Fig. 4), we would expect the hole wave function to be situated in the barrier. We attribute this effect to a kind of tunneling of the hole through the quantum disk, as a consequence of the very small disk radius. Note that this state continues to be the ground state and that the effect becomes even stronger for higher fields. Another consequence of this effect is a higher overlap of the electron and hole wave functions, which is an indication of type-I behavior.

In a next step, we studied the exciton properties as a function of the hole confinement potential, which allows us to explore the transition region from type-I systems ($V_h>0$) to type-II systems ($V_h<0$). Hereby we kept the disk radius fixed at $R=8$ nm. Figure 5 shows the phase diagram for the angular momentum transitions as a function of the confinement potential $V_h$ and the magnetic field $B$. A feature that immediately catches the eye is that up to $V_h\simeq-24.5$ meV the $l_h=0$ state remains the ground state over the total $B$ region under consideration. Investigating this more in depth, we find that, even for $B=0$ T, the hole wave function is located almost entirely inside the quantum disk. This is a consequence of the Hartree potential (due to the attraction to the electron) which overcomes the potential barrier of the disk. Therefore, we can speak of type-I systems up to $V_h\simeq-24.5$ meV.

In order to have a more physical idea of the origin of the type-I to type-II transition, we developed the following intuitive picture. When the system is type I, the hole will be located inside the quantum disk. This will happen when the effective potential [the sum of the hole confinement potential and the Hartree potential; i.e., $V_c(r_h)+V_h$ (see the inset of Fig. 4)] is lower at $r_h=0$ than at $r_h=R$. For a type-II sys-

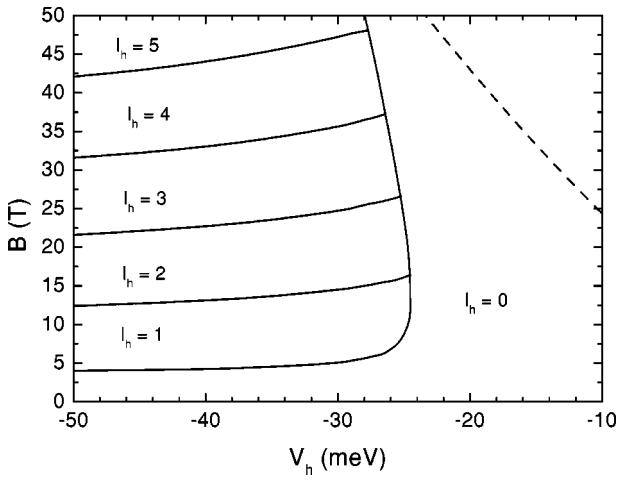


FIG. 5. Phase diagram of the successive $l_h$ states for varying confinement potential $V_h$, as a function of the magnetic field. The disk radius is fixed at $R=8$ nm. The dashed line indicates the result obtained by the approximate model.

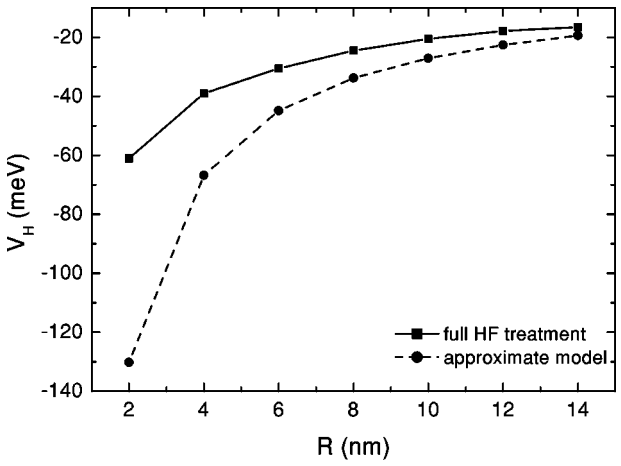


FIG. 6. Confinement potential of the hole at which a transition from a type-I to a type-II system occurs, as a function of the disk radius $R$. The solid curve (squared dots) indicates the result obtained within the HF treatment, whereas the dashed curve (circular dots) indicates the approximated result.

tem, however, the effective potential will be lower at the boundary, and the hole will prefer to sit outside the disk but near the boundary. Generally, we can state that the transition from type I to type II occurs when the effective potential at the origin equals the one at the radial boundary. Because we take the confinement potential zero inside the disk, this leads to the following formula:

$$V_c(r_h=0)=V_h+V_c(r_h=R). \tag{6}$$

From this equality, we can find an estimate for the confinement potential $V_h$ at which the type-I to type-II transition occurs. The Hartree potential was calculated within the approximation of an infinitely high electron confinement potential, where the electron wave function can be expressed by the Bessel functions $J_0$, i.e.,

$$V_c(r_h)=-\frac{e^2}{4\pi\epsilon}N^2\int\frac{|J_0(kr_e')|^2}{|r_h-r_e'|}d\mathbf{r}_e', \tag{7}$$

with $N^2=2/[R^2|J_1(kr_e')|^2]$ the normalization and $k=\sqrt{2m_eE}/\hbar$. In Fig. 6, we plot the values for $V_h$ as a function of the disk radius $R$ at which such a type-I to type-II transition occurs. We show the results obtained by the full Hartree-Fock calculation (solid curve, squared dots) and the approximated results, as obtained from Eq. (6) (dashed curve, circular dots). We find that for large $R$ the two curves converge to each other, but that for small $R$ an appreciable discrepancy exists. This is due to the fact that for small disk radii, the approximation of a hard wall confinement is less justified. By pushing the electron wave function completely into the disk (in contrast to the ''real'' case of a finite potential, where the wave function can tunnel into the barrier), the Hartree potential is strongly enhanced, thereby leading to a strong enhancement of the critical confinement potential $V_h$.

Another interesting property is the probability for recombination of the exciton. This is proportional to the square of the overlap integral[23]

$$I=\int\Psi_e(\mathbf{r})\Psi_h(\mathbf{r})d\mathbf{r}=\int_0^{2\pi}e^{i(l_e+l_h)}d\varphi\int_0^{\infty}\psi_e(r)\psi_h(r)rdr. \tag{8}$$

Notice that the first integral is equal to $2\pi\delta_{l_e+l_h}$, which means that the probability for de-excitation is only nonzero for the case $l_e+l_h=0$. This implies that after an angular momentum transition the probability for recombination of an exciton decreases drastically. In photoluminescence (PL) experiments, one will observe a strong quenching or even disappearance of the PL spectrum after a certain value of the magnetic field.

Figure 7 shows the overlap integral $I$ as a function of $V_h$, for $B=0$ T. Without a magnetic field, the $l_h=0$ state is always the ground state and, therefore, $I$ is nonzero over the total region. Up to $V_h=-25$ meV the overlap is large, and further increasing $-V_h$, we find a sudden strong decrease of

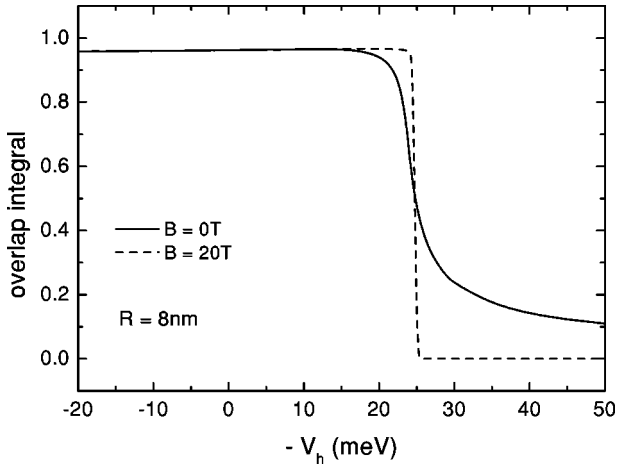


FIG. 7. Overlap integral for a varying confinement potential of the hole, for $R=8$ nm and at $B=0$ T (solid curve) and $B=20$ T (dashed curve).

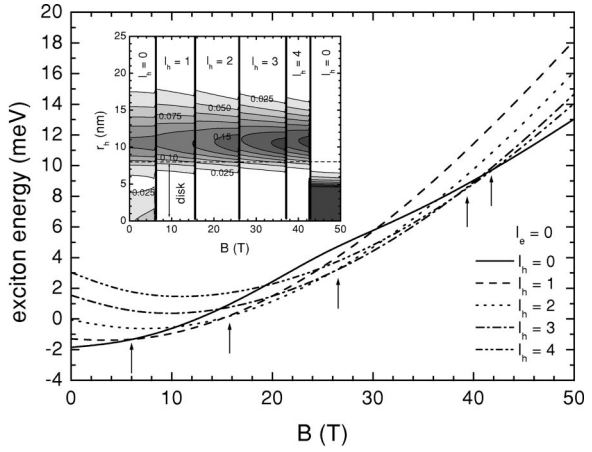


FIG. 8. Exciton ground-state energy for $V_h = -27$ meV. The successive $l_h$ states are indicated by arrows. Notice the reentrant behavior of the $l_h = 0$ state.

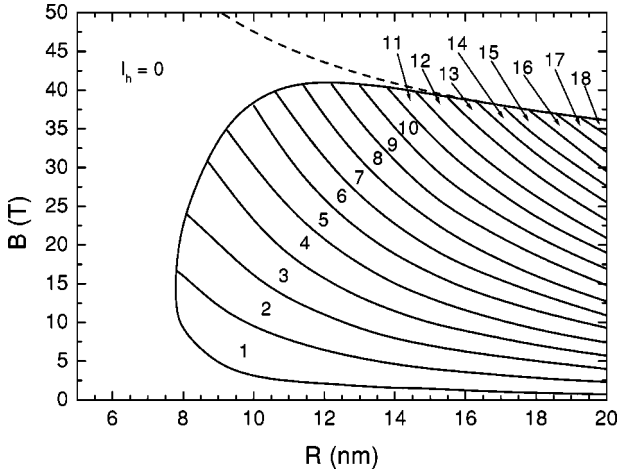


FIG. 9. $(B,R)$ Phase diagram for $V_h = -25$ meV. The reentrant behavior slowly decreases for large $R$. The dashed curve indicates the result obtained by the approximate model.

the overlap. The reason for this behavior is directly related to the position of the hole wave function. As long as the hole is sitting inside the disk, the overlap will be very large. However, from the moment the hole jumps outside the disk, the overlap decreases strongly. In fact, from Fig. 7 we can infer immediately the position of the hole. Furthermore, the region of the strong decrease in overlap indicates the transition from type-I to type-II behavior. The dashed line gives the overlap integral at $B = 20$ T. As we see from Fig. 5, a transition to the $l_h = 1$ state occurs when the confinement potential $V_h$ approaches $-24.5$ meV and the condition $l_e + l_h = 0$ for recombination of the exciton is no longer satisfied, which leads to $I = 0$. The recombination of the exciton will happen through indirect processes, resulting in a much longer lifetime of the exciton. The changing lifetime can be detected experimentally by a changing line shape.[27,28]

### C. Reentrant behavior

In this section, we concentrate more closely on the type-I to type-II transition region, i.e., $V_h$ between $-20$ and $-30$ meV. As an example, we investigated the exciton ground-state energy for $V_h = -27$ meV. The result is depicted in Fig. 8 which shows one additional remarkable feature: after several $l_h$ transitions with increasing magnetic field, we find at sufficiently large magnetic field, i.e., $B \simeq 42$ T, a reentrance of the $l_h = 0$ state. It is interesting also to take a look at the evolution of the wave function with increasing magnetic field. This is depicted as a contourplot in the inset of Fig. 8. Initially, for very small magnetic fields, we find that a small part of the wave function has already entered the dot region. However, at $B \simeq 6$ T, due to a jump to a higher angular momentum state, the hole wave function is pushed outside the dot region. Further increasing the magnetic field leads to more $l_h$ transitions, as we found already in Sec. III A. At the specific magnetic field value, however, where the re-entrance of $l_h = 0$ occurs, we find that suddenly the hole wave function jumps almost entirely inside the disk. At this point, the magnetic field and the attraction of the electron overcome the potential barrier of the quantum disk, and it will be energetically more favorable for the hole to sit inside the disk.

The reentrant behavior is also visible in the $(B,V_h)$ phase diagram (Fig. 5). We want to emphasize that there will be a reentrant behavior for any value of $V_h < -24.5$ meV, for sufficiently large magnetic fields. This can already be seen from Fig. 5, where the line which indicates the transition from a certain $l_h$ state to the $l_h = 0$ state is not a straight vertical line, but has a small slope. For example for $V_h = -50$ meV we found that a magnetic field of $B = 193$ T is needed to induce this reentrance to the $l_h = 0$ state.

Another question which arises is how the disk radius influences the reentrant behavior. In our previous investigation of the influence of the disk radius on the ground-state energy, we found no evidence of this, because we did not consider large enough magnetic fields for the confinement potential under consideration ($V_h = -50$ meV). Therefore, we decided to make a new $(B,R)$ phase diagram, this time for $V_h = -25$ meV, for which we know from Fig. 5 that reentrant behavior occurs at rather small magnetic fields. The result is depicted in Fig. 9, and the first striking feature is that the reentrant behavior occurs for any disk with radius $R > 8$ nm. Furthermore, we find more $l_h$ transitions for larger disk radii, thereby increasing the magnetic field at which the reentrance of $l_h = 0$ takes place. However, at $R \simeq 12$ nm, we find that the magnetic field position of the reentrant behavior reaches a maximum value $B \simeq 42$ T. For larger disk radii, the reentrance occurs at slightly decreasing magnetic field. Indeed, with increasing disk radius, the electron and hole are drawn more and more apart, and therefore it will sooner become energetically more favorable for the hole to jump inside the disk.

This reentrant behavior can be understood qualitatively from the following simple model. We compare the approximate energies for a hole of respectively a type-II and a type-I system:

$$E_h^{II} = \frac{3}{2}\hbar\omega_{c,h} - \frac{e^2}{4\pi\epsilon_0\epsilon}\frac{1}{R} - V_h, \tag{9a}$$

$$E_h^I = \frac{1}{2}\hbar\omega_{c,h} - E_{Coulomb}. \tag{9b}$$

The approximate energy for a hole in a type-II system [Eq. (9a)] is constructed by approximating the disk (with radius $R$) by an infinitely high barrier for the hole. The first term of Eq. (9a) gives the one-particle energy of the hole, which is just the first energy level of a particle in a magnetic field which fulfills the zero-wave-function condition at the disk boundary. The second term is the Coulomb interaction between the electron and hole, and the third is the potential energy of the hole. In a type-I system [Eq. (9b)] both the electron and hole are located inside the disk and are subjected to a magnetic field. Now the one-particle hole energy is just the energy of the first Landau level. We approximated the Coulomb energy [second term in Eq. (9b)] by using the single-particle wave function of the electron and hole. At strong magnetic fields and for large disk radii, i.e., $R > l_B$, the potential confinement by the disk can be neglected with regard to the confinement by the magnetic field. The single-particle wave functions are then the well-known wave functions of a particle in a magnetic field, given by

$$\varphi_{e,h}(\mathbf{r}_{e,h}) = \sqrt{\frac{1}{\pi}}\frac{1}{\sqrt{2}l_B}\exp\left(-\frac{r_{e,h}^2}{4l_B^2}\right), \tag{10}$$

for the ground state ($n=0, l_h=0$). As the wave functions are mass independent, there is no distinction between the electron and hole. Therefore we can treat our system as being completely analogous to a system consisting of two electrons in a magnetic field, for which our first-order approximation of the Coulomb interaction energy can be calculated analytically and which reduces to

$$E_{Coul} = \frac{e^2}{4\pi\epsilon_0\epsilon}\frac{\sqrt{\pi}}{2}\sqrt{\frac{e}{\hbar}}\sqrt{B} \tag{11a}$$

$$= C_{coul}\sqrt{B}. \tag{11b}$$

Equalization of Eqs. (9a) and (9b) gives us the magnetic field at which the reentrance occurs as a function of both disk radius $R$ and confinement potential $V_h$. The transition magnetic field can be obtained analytically as

$$B = \frac{m_h^2}{2e^2\hbar^2}C_{coul}\left[C_{coul} - \sqrt{C_{coul}^2 + \frac{4e\hbar}{m_h}\left(\frac{e^2}{4\pi\epsilon_0\epsilon}\frac{1}{R} + V_h\right)}\right] + \frac{m}{e\hbar}\left(\frac{e^2}{4\pi\epsilon_0\epsilon}\frac{1}{R} + V_h\right). \tag{12}$$

For a fixed radius $R$, we can vary $V_h$ and deduce the magnetic field at which the transition occurs. The result is shown by the dashed curve in Fig. 5. For large fields, the approximated curve (dashed line) has qualitatively the same behavior as the curve obtained from the full Hartree-Fock treatment and the two curves converge to each other. The result for a fixed $V_h$, when varying the disk radius $R$, is shown by the dashed curve in Fig. 9. We find a perfect agreement for large disk radii, where our model is valid. The discrepancy for small disk radii is a consequence of our assumption to neglect the disk confinement.

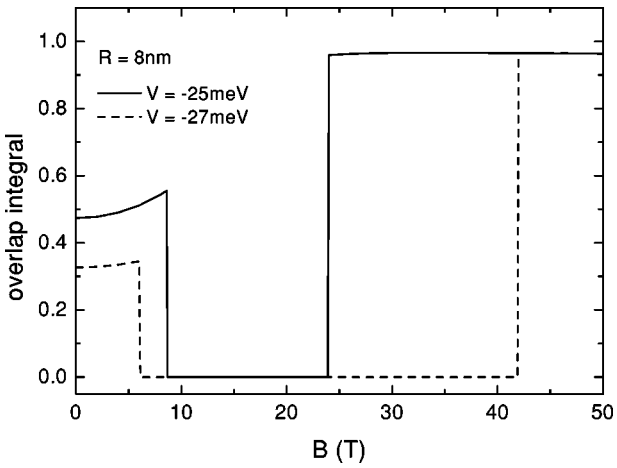


FIG. 10. Overlap integral as a function of the magnetic field, for fixed $R=8$ nm and for $V_h=-25$ meV (solid curve) and $V_h=-27$ meV (dashed curve). When $l_e+l_h\neq 0$, the overlap is 0.

Figure 10 shows the overlap integral $I$ as a function of the magnetic field for confinement potentials of the hole, $V_h=-25$ meV (solid curve) and $V_h=-27$ meV (dashed curve), and a fixed disk radius $R=8$ nm. At first we find a slowly increasing overlap, which is a consequence of the increasing magnetic field, pushing the particles closer together. The already rather large value of the overlap indicates that a considerable part of the hole is already situated inside the disk. When the first $l_h$ transition occurs, the overlap falls immediately down to zero, because $l_e+l_h\neq 0$. The overlap remains zero, until the $l_h=0$ state returns as the ground state and the condition $l_e+l_h=0$ is satisfied. This reentrance of $l_h=0$ is accompanied by a jump of the wave function in the disk, and this leads to the strong enhancement of the overlap value. We see that the reentrance of the $l_h=0$ state happens at lower magnetic fields for the lower potential barrier.

Figure 11 shows the overlap integral $I$ as a function of the disk radius $R$ for $B=0$ T (solid curve), $B=20$ T (dashed curve), and $B=40$ T (dotted curve). This figure gives evidence for the fact that for very small radii the hole wave function is almost entirely situated inside the disk. For increasing disk radius, the hole is pushed more and more outside the disk, thereby decreasing the value of the overlap integral. This decrease is initially less for increasing magnetic field because of the enhanced localization effect. For sufficiently large magnetic fields, $l_h$ transitions are induced, which leads to a zero overlap integral. Also here we see that for sufficient large $R$ a reentrant behavior to the $l_h=0$ state is found, at which point the overlap integral becomes again nonzero.

### D. Excitation spectrum

Last, we investigated the exciton energy spectrum as a function of the magnetic field. The physical parameters used in this calculation are the ones mentioned in Sec. II, with a disk radius $R=8$ nm. We considered states with different

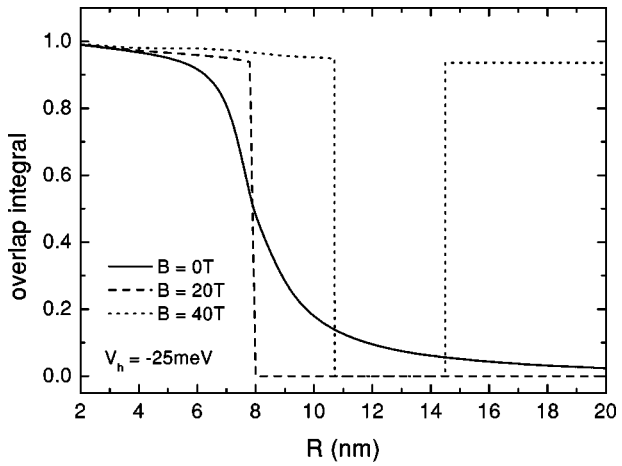


FIG. 11. Overlap integral as a function of the disk radius, for $V_h=-25$ meV and magnetic fields of respectively 0 T (solid curve), 20 T (dashed curve) and 40 T (dotted curve).

radial quantum numbers $k_e$ and $k_h$ and different angular momenta $l_e$ and $l_h$. Note that $k_e$ and $k_h$ are approximate quantum numbers for the current system. Furthermore, our results are a *first-order* perturbation theory approximation to the real energy spectrum, as we perform only one HF iteration; i.e., the energy of the exciton is obtained by solving the equation for the hole in the field of the confined electron. Note that changing the electron quantum number results in a strong increase of the energy value. The states $(k_e,l_e)=(2,0)$ and $(1,\pm 2)$ appear to be already unbound; i.e., the energy exceeds the electron barrier of 250 meV. The inset of Fig. 12(a) shows the bound states of the energy spectrum where we varied both $k_e$ and $l_e$, keeping $k_h$ and $l_h$ fixed at (0,0). The main part of Fig. 12(a) shows the energy spectrum for fixed $(k_e,l_e)=(0,0)$ and varying the hole quantum numbers $k_h$ and $l_h$. We find that now the energy values span a smaller energy region. This is due to the fact that (i) the hole is much heavier than the electron and therefore has substantially lower energies and (ii) the hole is less confined. In fact, for every possible value of the electron quantum numbers $k_e$ and $l_e$, one has a spectrum of all possible $(k_h,l_h)$ values, and because these span a smaller energy region, the total energy spectrum will consist of mainly the electron branches, with superimposed on each of them the spectrum with the changing hole quantum numbers.

Notice also the anomalous behavior of certain states, e.g., $(k_h,l_h)=(2,0)$, in the high-magnetic-field region. To investigate this further, we concentrated on the variation of the radial quantum number $k_h$, keeping the angular momentum $l_h$ fixed at 0. This result is shown in Fig. 12(b) which clearly shows the occurrence of anticrossings. These anticrossings are due to the fact that the radial quantum number is not a good quantum number, leading to strong mixing of radial states at the anticrossings.

## IV. CONCLUSIONS

We investigated the exciton properties in a strongly simplified type-II model quantum disk, with the hole located in the barrier. Strain effects were disregarded and a flat disk geometry was assumed. Because in our model system there is no geometrical confinement for the hole, the only ''confinement'' comes from the attraction to the electron, i.e., the Coulomb interaction energy. We solved this problem by using a Hartree-Fock mesh calculation, which allowed us to calculate the exciton energy, without an *a priori* knowledge of the single-particle hole wave function.

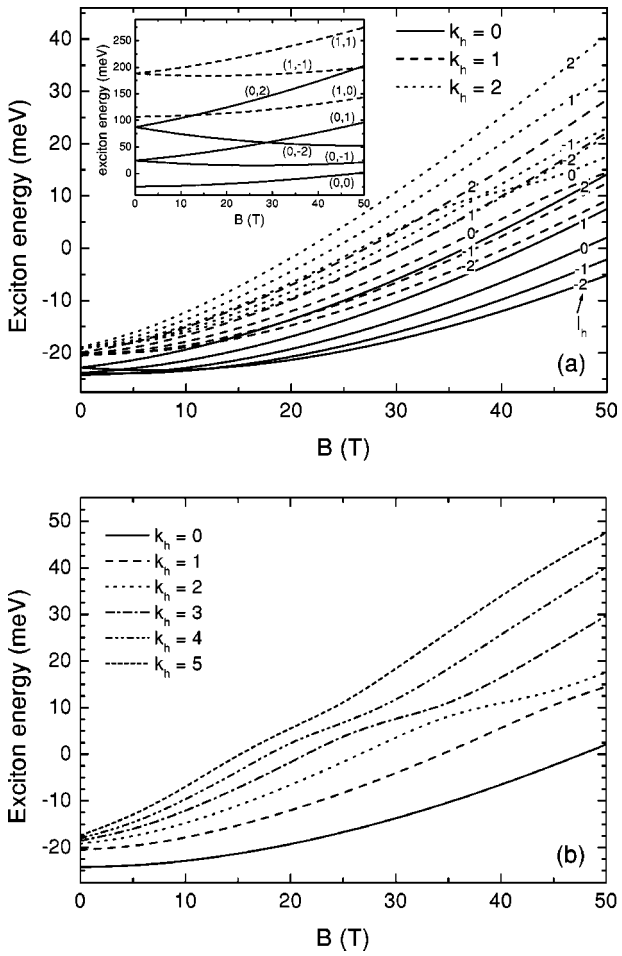


FIG. 12. (a) Energy spectrum for different $k_h$ and $l_h$, for fixed $(k_e,l_e)=(0,0)$, as a function of the magnetic field. Inset: the same, but now for different $k_e$ and $l_e$ and for $(k_h,l_h)=(0,0)$. (b) The same as in (a), but now for $l_h=0$. Notice the anticrossings as a function of the magnetic field, which is due to the lifting of the degeneracy or a strong mixing of the radial states.

We studied the influence of a perpendicular applied magnetic field and found *angular momentum transitions* with increasing magnetic field. These are a consequence of the fact that the magnetic field pushes the hole closer to the disk, making it energetically more favorable to jump to a higher $l_h$ state. Varying the disk radius showed that the transitions shift to lower magnetic field for larger $R$. We also found that the hole is located almost entirely inside the disk for very small disk radii.

Furthermore, we investigated the transition region from *type-I to type-II* systems by varying the confinement potential of the hole, $V_h$. A striking feature here is the fact that we are dealing with type-I systems up to $V_h>-24.5$ meV.

Even at $B=0$ T, the Coulomb attraction overcomes the potential barrier and the hole is situated inside the quantum disk. Taking a closer look at the transition region between type I and type II showed the existence of a *reentrant behavior* of the $l_h=0$ state. This reentrant behavior is coupled with a sudden jump of the wave function into the disk.

The angular momentum transitions and the reentrant behavior should be measurable experimentally by quenching of luminescence and/or changing line shapes.

In the last part, we studied the excitation spectrum as a function of the magnetic field. We varied the quantum numbers $k$ and $l$ for both electron and hole, and found that for every value of $(k_e,l_e)$ one has a spectrum consisting of the different radial and angular momentum hole states. Furthermore, taking a closer look at the varying $k_h$ states, with fixed $l_h$ and fixed electron quantum numbers, we found an anticrossing of levels, a consequence of the fact that $k_h$ is not a good quantum number and therefore lifts the degeneracy.

## ACKNOWLEDGMENTS

K.L.J. was supported by the ''Instituut voor de aanmoediging van Innovatie door Wetenschap en Technologie in Vlaanderen'' (IWT-Vl) and B.P. is a post-doctoral researcher with the Flemish Science Foundation (FWO-Vl). Discussions with M. Hayne, M. Tădić, and A. Matulis are gratefully acknowledged. Part of this work was supported by the FWO-Vl, IUAP-IV, the ''Bijzonder Onderzoeksfonds van de Universiteit Antwerpen'' (GOA), and the EC-project NANOMAT.

## APPENDIX: CALCULATION OF THE HARTREE INTEGRAL

The Hartree integral, which expresses the effect of one particle, e.g., the electron, on the other particle, e.g., the hole, is given by

$$\int \frac{\rho(r')}{|\mathbf{r}-\mathbf{r}'|}d\mathbf{r}' = \int dr'r' \int d\varphi' \frac{\rho(r')}{\sqrt{r^2+r'^2-2rr'\cos(\varphi-\varphi')}}. \tag{A1}$$

As we are dealing with cylindrical symmetry, we can remove the $\varphi$ dependence. The integral over the angle becomes the complete elliptic integral of the first kind, which converts Eq. (A1) into

$$4\int \frac{\rho(r')r'}{r+r'}\mathcal{K}\left(\frac{4rr'}{(r+r')^2}\right)dr'. \tag{A2}$$

The radial integral has to be solved numerically. We use a polynomial approximation for the elliptic function,[26] namely,

$$\mathcal{K}(x)=[a_0+a_1x'+a_2x'^2]-[b_0+b_1x'+b_2x'^2]\ln(x'), \tag{A3}$$

with $x'=1-x$ and where the coefficients $a_i$ and $b_i$ are given in Ref. 26. Since this implies the appearance of a logarithmic divergence in the integrand, the commonly used trapezoidal rule will give bad results. Therefore we used another method, the so-called ''logarithmically weighted method,'' which takes into account this problem.

Generally, the following integral can be considered:

$$I(r)=\int_0^1 dxF(x)\ln\frac{(x-r)^2}{(x+r)^2}, \tag{A4}$$

which, after transformation, becomes

$$I(r)=\sum_{i=0}^{N-1}\int_0^h dxF(x+hi)\ln\frac{[x-(r-hi)]^2}{[x+(r+hi)]^2}, \tag{A5}$$

with $h$ the discretization step and $N$ the number of steps. If we replace $F(x+hi)$ by $F_i+[F_{i+1}-F_i](x/h)$, we can write Eq. (A5) as

$$I(r)=\sum_{i=0}^{N-1}\{F_iA_i(r)+[F_{i+1}-F_i]C_i(r)\}, \tag{A6}$$

and the remaining problem is the calculation of the coefficients $A_i(r)$ and $C_i(r)$. The integrals which determine the coefficients can be solved exactly, which leads to the following results:

$$A_i(r)=a[h-(r-hi)]-a[h+(r+hi)], \tag{A7}$$

with

$$a(y)=2y\ln y+2(h-y)\ln(h-y) \tag{A8}$$

and

$$C_i(r)=h^{-1}\{c[h-(r-hi)]-c[h+(r+hi)]\}-2r, \tag{A9}$$

with

$$c(y)=[y(2h-y)]\ln y+(h-y)^2\ln(h-y). \tag{A10}$$

*Electronic address: karenj@uia.ua.ac.be
†Electronic address: bpartoen@uia.ua.ac.be
‡Electronic address: peeters@uia.ua.ac.be

[1] For a review, see, e.g., D. Bimberg, M. Grundmann, and N.N. Ledentsov, *Quantum Dot Heterostructures* (Wiley, Chichester, 1999).
[2] D.J. Eaglesham and M. Cerullo, Phys. Rev. Lett. **64**, 1943 (1990).
[3] C.W. Snyder, B.G. Orr, D. Kessler, and L.M. Sander, Phys. Rev. Lett. **66**, 3032 (1991).
[4] D. Leonard, M. Krishnamurthy, C.M. Reaves, S.P. Denbaars, and P.M. Petroff, Appl. Phys. Lett. **63**, 3203 (1993).
[5] J.M. Moison, F. Houzay, F. Barthe, L. Leprince, E. André, and O.

Vatel, Appl. Phys. Lett. **64**, 196 (1994).
[6] P.D. Wang, J.L. Merz, S. Fafard, R. Leon, D. Leonard, G. Medeiros-Ribeiro, M. Oestreich, P.M. Petroff, K. Uchida, N. Miura, H. Akiyama, and H. Sakaki, Phys. Rev. B **53**, 16 458 (1996).
[7] A. Polimeni, S.T. Stoddart, M. Henini, L. Eaves, P.C. Main, K. Uchida, R.K. Hayden, and N. Miura, Physica E (Amsterdam) **2**, 662 (1998).
[8] U. Bockelmann, W. Heller, and G. Abstreiter, Phys. Rev. B **55**, 4469 (1997).
[9] M. Bayer, A. Schmidt, A. Forchel, F. Faller, T.L. Reinecke, P.A. Knipp, A.A. Dremin, and V.D. Kulakovskii, Phys. Rev. Lett. **74**, 3439 (1995).
[10] L.R. Wilson, D.J. Mowbray, M.S. Skolnick, M. Morifuji, M.J. Steer, I.A. Larkin, and M. Hopkinson, Phys. Rev. B **57**, R2073 (1998).
[11] O. Stier, M. Grundmann, and D. Bimberg, Phys. Rev. B **59**, 5688 (1999).
[12] M. Brasken, M. Lindberg, D. Sundholm, and J. Olsen, Phys. Rev. B **61**, 7652 (2000).
[13] W. Xie, Physica B **279**, 253 (2000).
[14] J. Song and S.E. Ulloa, Phys. Rev. B **52**, 9015 (1995).
[15] K.L. Janssens, F.M. Peeters, and V.A. Schweigert, Phys. Rev. B **63**, 205311 (2001).
[16] S. Nomura, L. Samuelson, M.-E. Pistol, K. Uchida, N. Miura, T. Sugano, and Y. Aoyagi, Appl. Phys. Lett. **71**, 2316 (1997).
[17] M. Hayne, R. Provoost, M.K. Zundel, Y.M. Manz, K. Eberl, and V.V. Moshchalkov, Phys. Rev. B **62**, 10 324 (2000).
[18] M. Sugisaki, H.-W. Ren, K. Nishi, S. Sugou, T. Okuno, and Y. Masumoto, Physica B **256–258**, 169 (1998).
[19] F. Hatami, M. Grundmann, N.N. Ledentsov, F. Heinrichsdorff, R. Heitz, J. Böhrer, D. Bimberg, S.S. Ruvimov, P. Werner, V.M. Ustinov, P.S. Kop'ev, and Zh.I. Alferov, Phys. Rev. B **57**, 4635 (1998).
[20] C. Pryor, M.-E. Pistol, and L. Samuelson, Phys. Rev. B **56**, 10 404 (1997).
[21] S. Nomura, L. Samuelson, C. Pryor, M.-E. Pistol, M. Stopa, K. Uchida, N. Miura, T. Sugano, and Y. Aoyagi, Phys. Rev. B **58**, 6744 (1998).
[22] Ph. Lelong, K. Suzuki, G. Bastard, H. Sakaki, and Y. Arakawa, Physica E (Amsterdam) **7**, 393 (2000).
[23] A.B. Kalameitsev, V.M. Kovalev, and A.O. Govorov, JETP Lett. **68**, 669 (1998).
[24] M.V. Ivanov, J. Phys. B **27**, 4513 (1994); M.V. Ivanov and P. Schmelcher, Phys. Rev. A **61**, 022505 (2000).
[25] F.M. Peeters and V.A. Schweigert, Phys. Rev. B **53**, 1468 (1996).
[26] *Handbook of Mathemetical Functions*, edited by M. Abramowitz and I. A. Stegun, Natl. Bur. Stand. Appl. Math. Ser. No. 55 (U.S. GPO, Washington, D.C., 1970), expression 17.3.34.
[27] T. Yasuhira, K. Uchida, N. Miura, E. Kurtz, and C. Klingshirn (unpublished).
[28] E.F. Schubert and W.T. Tsang, Phys. Rev. B **34**, 2991 (1986).